

Scattering resonances and pairing in a Rabi-coupled Fermi gas

Olivier Bleu,^{1,*} Brendan C. Mulkerin,^{1,*} Cesar R. Cabrera,^{2,3} Jesper Levinsen,¹ and Meera M. Parish¹

¹*School of Physics and Astronomy, Monash University, Victoria 3800, Australia*

²*Institute for Quantum Physics, Universität Hamburg, Luruper Chaussee 149, 22761 Hamburg, Germany*

³*The Hamburg Centre for Ultrafast Imaging, Universität Hamburg, Luruper Chaussee 149, 22761 Hamburg, Germany*

(Dated: March 17, 2025)

We investigate the possibility of using a Rabi drive to tune the interactions in an atomic Fermi gas. Specifically, we consider the scenario where two fermion species (spins) are Rabi coupled and interacting with a third uncoupled species. Using an exact calculation within a minimal low-energy model, we derive analytical expressions for the effective scattering length and effective range that characterize the collisions between a Rabi-dressed atom and an atom from the third species. In particular, we find that new scattering resonances emerge in the Rabi-coupled system, which we demonstrate are linked to the existence of hybrid two-body bound states. Furthermore, we show via a generalized Thouless criterion that the scattering properties have a direct impact on the superfluid transitions in the Rabi-coupled Fermi gas. The presence of Rabi-induced resonances thus has implications for the investigation of many-body physics with driven atomic gases.

The Feshbach resonance is a cornerstone of ultracold atomic gas experiments [1]. By tuning a molecular two-body bound state into resonance using, e.g., an external magnetic field, the interatomic collisions can be precisely controlled, thus providing an essential tool for simulating correlated quantum phenomena [2]. This has permitted the experimental realization of a range of many-body systems, including paired-fermion superfluids [3–6] and polaron quasiparticles [7–10], as well as exotic few-body states such as Efimov trimers [11, 12].

Another important component of the cold-atom toolbox is the ability to manipulate atoms with electromagnetic fields. In particular, the coupling of two atomic species using radio, microwave or optical frequency pulses has provided a powerful spectroscopic probe of the state of an atomic gas, both in the frequency and the time domains [13–15]. Even in the case of a continuous drive, which goes beyond the linear response regime, the resulting Rabi oscillations can yield information about quantum behavior such as the superfluid order parameter in a Bose Einstein condensate (BEC) [16] or Landau quasiparticle properties in a Fermi gas [17–21]. Most recently, there is the exciting prospect of using a Rabi drive to fundamentally modify the quantum gas itself, a situation which has already been achieved in two-component Bose mixtures [22–28] and for a highly spin-imbalanced Fermi gas [29].

In this work, we combine these two concepts and investigate the effect of a strong Rabi drive on the interactions in a Fermi gas. Specifically, we consider a system where two hyperfine states of the same atom are coupled via a coherent drive, as illustrated in Fig. 1(a), and the resulting dressed state is interacting with another hyperfine state or atomic species. This scenario thus requires three distinct states, although a strong coupling can effectively reduce it to a two-component system. Three-component

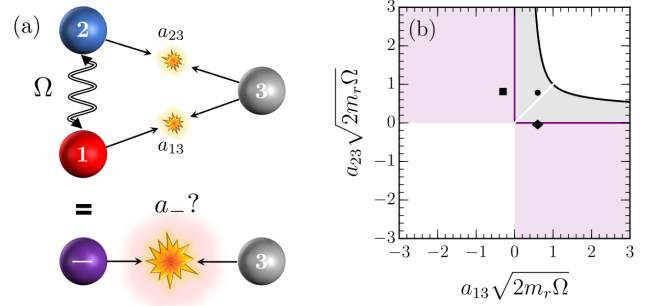


Figure 1. (a) Sketch of the system considered. A coherent drive of strength Ω couples two atomic species (blue and red), which gives rise to dressed particles (purple). Both of the Rabi coupled species can interact with a third component (gray) via short range interactions that are characterized by the scattering lengths a_{13} and a_{23} . The resulting effective scattering length a_- for the lowest energy dressed particle can exhibit resonances. (b) Existence diagram of the dressed Feshbach resonances. The purple-shaded area indicates where a single resonance exists when varying the detuning of the Rabi drive, while in the gray area two resonances exist. By contrast, no resonances exist in the white areas, including along the diagonal where $a_{13} = a_{23}$. Here, m_r is the reduced mass of the coupled and uncoupled components.

Fermi gases have been experimentally realized with ^6Li atoms [12, 30–33], and there are theoretical studies suggesting that radiofrequency (rf) radiation can be used to manipulate Feshbach resonances in this system [34, 35]. However, the previous calculations have all involved a multi-channel formulation, whereas here we use a minimal low-energy description which clearly exposes the key physics and allows us to extract analytic two-body parameters that can straightforwardly be applied to the many-body system.

Focusing on the scattering properties of the lowest-

energy Rabi-dressed atom and an undriven atom [Fig. 1(a)], we obtain an exact analytic expression for the effective scattering length characterizing this process, and we find that it can exhibit resonances for a wide range of parameters [Fig. 1(b)]. Furthermore, we show that the resonances are linked to the emergence of hybrid two-body bound states, whose composition are strongly influenced by the drive. Our results thus demonstrate that the Rabi drive can significantly alter the two-body interactions, and in particular that resonances can be accessed purely by changing the parameters of the drive. A key advantage of the Rabi-drive-induced interactions over conventional magnetically tunable Feshbach resonances is that it gives access to an additional observable—the pseudospin of the coupled atoms—which can be used to monitor both few- and many-body physics.

Exploiting the control of two-body interactions, we investigate the influence on the pairing instability—a precursor to the superfluid transition—in the Rabi-coupled Fermi gas. Within the Thouless criterion [36, 37], we find that one can achieve a crossover between different pairing regimes purely by varying the detuning of the Rabi drive, and we reveal an excited many-body branch which may be dynamically accessible in an out-of-equilibrium experiment.

Model and T matrix.— We model the Rabi-coupled Fermi system depicted in Fig. 1(a) with the Hamiltonian

$$\hat{H} = \hat{H}_0 + \hat{V}_1 + \hat{V}_2, \quad (1)$$

where

$$\hat{H}_0 = \sum_{\mathbf{k}, j} \epsilon_{\mathbf{k}j} \hat{f}_{\mathbf{k}j}^\dagger \hat{f}_{\mathbf{k}j} + \frac{\Omega}{2} \sum_{\mathbf{k}} (\hat{f}_{\mathbf{k}1}^\dagger \hat{f}_{\mathbf{k}2} + h.c.), \quad (2a)$$

$$\hat{V}_j = g_{j3} \sum_{\mathbf{k}, \mathbf{k}', \mathbf{q}} \hat{f}_{\mathbf{k}+\mathbf{q}j}^\dagger \hat{f}_{\mathbf{k}j} \hat{f}_{\mathbf{k}'-\mathbf{q}3} \hat{f}_{\mathbf{k}'3}. \quad (2b)$$

Here, $\hat{f}_{\mathbf{k}j}$ ($\hat{f}_{\mathbf{k}j}^\dagger$) are annihilation (creation) operators for fermions of species $j = \{1, 2, 3\}$ with momentum \mathbf{k} , and $\epsilon_{\mathbf{k}j}$ the corresponding kinetic energies. In the following, we take $\epsilon_{\mathbf{k}1} \equiv \epsilon_{\mathbf{k}} = k^2/2m$, $\epsilon_{\mathbf{k}2} = \epsilon_{\mathbf{k}} + \delta$ and $\epsilon_{\mathbf{k}3} = k^2/2m_3$. Here, δ encodes the detuning of the Rabi drive frequency with respect to the 1-2 transition, and Ω is the strength of the coupling, where we have used the rotating wave approximation. We have also defined different masses m and m_3 of the two coupled species and species 3, respectively, which allows us to investigate general mixtures. Finally, g_{j3} corresponds to the “bare” strength of the contact interactions between species j and 3. The bare couplings are related to the corresponding s -wave scattering lengths a_{j3} via $\frac{1}{g_{j3}} = \frac{m_r}{2\pi a_{j3}} - \sum_{\mathbf{k}}^{\Lambda} \frac{1}{\epsilon_{\mathbf{k}} + \epsilon_{\mathbf{k}3}}$ with reduced mass $m_r = mm_3/(m + m_3)$, as well as an ultraviolet cutoff Λ which will eventually be sent to infinity at the end of the calculation. Throughout, we work in units in which the volume, the reduced Planck constant, and Boltzmann’s constant are all 1.

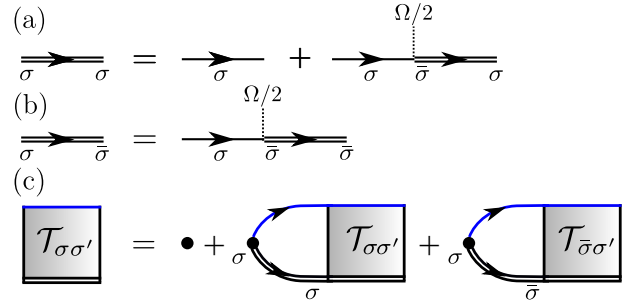


Figure 2. (a) Diagonal $G_{\sigma\sigma}$ and (b) off-diagonal $G_{\sigma\bar{\sigma}}$ ($\bar{\sigma} \neq \sigma$) single-particle Green’s functions for species $\sigma = \{1, 2\}$ in the presence of a Rabi drive. The thin solid lines represent the bare Green’s functions in the absence of Rabi drive, the vertical dotted lines illustrate the Rabi coupling between species 1 and 2, and the double lines represent the Rabi-dressed Green’s functions. (c) Diagrammatic representation of the T -matrix equation, where the circle represents the interaction vertex $g_{\sigma 3} \delta_{\sigma\sigma'}$, and the thin blue line is the Green’s function of a particle from species 3.

The noninteracting part of the Hamiltonian can be diagonalized as

$$\hat{H}_0 = \sum_{\mathbf{k}, \pm} (\epsilon_{\mathbf{k}} + \epsilon_{\pm}) \hat{f}_{\mathbf{k}\pm}^\dagger \hat{f}_{\mathbf{k}\pm} + \sum_{\mathbf{k}} \epsilon_{\mathbf{k}3} \hat{f}_{\mathbf{k}3}^\dagger \hat{f}_{\mathbf{k}3}. \quad (3)$$

The dressed particle operators are related to the bare operators via

$$\begin{pmatrix} \hat{f}_{\mathbf{k}-} \\ \hat{f}_{\mathbf{k}+} \end{pmatrix} = \begin{pmatrix} c & -s \\ s & c \end{pmatrix} \begin{pmatrix} \hat{f}_{\mathbf{k}1} \\ \hat{f}_{\mathbf{k}2} \end{pmatrix}, \quad (4)$$

where the transformation coefficients satisfy $c^2 = \frac{1}{2}(1 + \frac{\delta}{\sqrt{\delta^2 + \Omega^2}})$, $cs = \frac{\Omega}{2\sqrt{\delta^2 + \Omega^2}}$, and $c^2 + s^2 = 1$. The dressed single-particle kinetic energies are now shifted parabolas $\epsilon_{\mathbf{k}} + \epsilon_{\pm}$, with $\epsilon_{\pm} = \frac{1}{2}(\delta \pm \sqrt{\delta^2 + \Omega^2})$. Since the single-particle states of species 1 and 2 are no longer eigenstates of the non-interacting Hamiltonian, the corresponding single-particle Green’s functions

$$G_{\sigma\sigma'}(\mathbf{k}, \omega) = \langle 0 | \hat{f}_{\mathbf{k}\sigma'}(\omega - \hat{H}_0 + i0)^{-1} \hat{f}_{\mathbf{k}\sigma}^\dagger | 0 \rangle, \quad (5)$$

with $\sigma, \sigma' = \{1, 2\}$, are not diagonal and depend on the Rabi drive (the factor $+i0$ shifts poles infinitesimally into the lower half plane). The diagrams corresponding to the Rabi-dressed Green’s functions are presented in Fig. 2(a,b). By contrast, the third species is unaffected by the Rabi drive and thus its single-particle Green’s function is simply given by $G_3(\mathbf{k}, \omega) = (\omega - \epsilon_{\mathbf{k}3} + i0)^{-1}$.

We now turn to the interactions between an atom of species 3 with a Rabi-coupled atom, Fig. 1(a). Although the form of \hat{V} does not include direct interactions between species 1 and 2, the Rabi-induced interconversion processes discussed above must be accounted for, since it can couple bound and scattering states. As a result, we

find that the two-body T -matrix that describes the interactions can be conveniently written as a 2×2 matrix equation of the form

$$\mathbf{T}(\omega) = \mathbf{g} + \mathbf{g}\mathbf{\Pi}(\omega)\mathbf{T}(\omega), \quad (6)$$

as illustrated in Fig. 2(c). In the basis of the pseudospins of species 1 and 2, we have

$$\mathbf{g} = \begin{pmatrix} g_{13} & 0 \\ 0 & g_{23} \end{pmatrix}, \quad \mathbf{\Pi}(\omega) = \begin{pmatrix} \Pi_{11}(\omega) & \Pi_{12}(\omega) \\ \Pi_{21}(\omega) & \Pi_{22}(\omega) \end{pmatrix}, \quad (7)$$

and the functions $\Pi_{\sigma\sigma'}(\omega)$ are related to the single-particle Green's functions as

$$\Pi_{\sigma\sigma'}(\omega) = \int \frac{d\omega'}{2i\pi} \sum_{\mathbf{q}} G_{\sigma\sigma'}(-\mathbf{q}, -\omega') G_3(\mathbf{q}, \omega + \omega'). \quad (8)$$

Inverting (6) gives $\mathbf{T}(\omega) = [\mathbf{g}^{-1} - \mathbf{\Pi}(\omega)]^{-1}$, and the elements of the matrix can be evaluated analytically — for details, see the Supplemental Material (SM) [38].

Rabi-drive-induced Feshbach resonances.— We now demonstrate how the application of a strong Rabi drive can lead to scattering resonances that can be accessed purely by varying the parameters of the drive, such as the detuning, rather than by varying a magnetic field as in conventional Feshbach resonances. To this end, we consider the elastic scattering between a lower dressed particle $\hat{f}_{\mathbf{k}-}^\dagger$ and a particle in the third component (as we explain below, scattering involving the upper dressed state does not lead to a resonance). Naively, one might expect that the effective scattering length for this process is given by a weighted sum of the bare scattering lengths of the form $a_{13}c^2 + a_{23}s^2$, which only features a resonance if one of the bare scattering lengths is resonant. Indeed, this approximation works well when one considers weakly interacting Bose gases [24, 26, 39]. However, it neglects the interconversion between species 1 and 2 during the scattering process, as well as the shift of the single-particle continuum. The possibility of resonances depends on the non-trivial interplay between these effects.

To obtain the scattering T matrix between the lower dressed state and an atom of species 3, we rotate into the dressed-state basis which gives $T_-(\omega) = c^2\mathbf{T}_{11}(\omega) + s^2\mathbf{T}_{22}(\omega) - 2cs\mathbf{T}_{12}(\omega)$, where we have used $\mathbf{T}_{21}(\omega) = \mathbf{T}_{12}(\omega)$. In the limit of small collision energy $\epsilon_{\mathbf{k}} + \epsilon_{\mathbf{k}3}$, measured from the shifted continuum ϵ_- , this can be expanded as

$$T_-^{-1}(\epsilon_- + \epsilon_{\mathbf{k}} + \epsilon_{\mathbf{k}3}) \simeq \frac{m_r}{2\pi} \left(\frac{1}{a_-} - r_{\text{eff}} \frac{k^2}{2} + ik \right), \quad (9)$$

where we have introduced the dressed scattering length a_- and the effective range r_{eff} . We find that these can

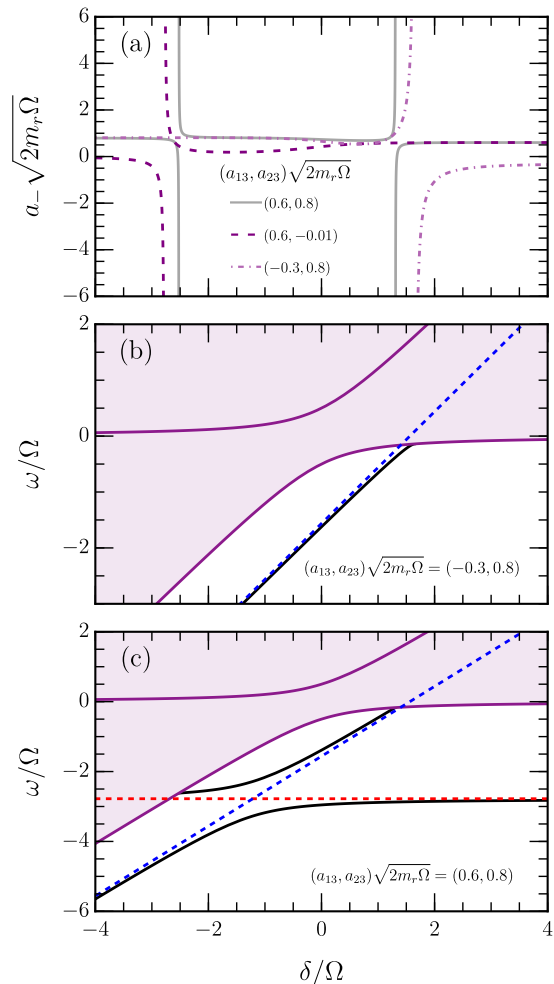


Figure 3. Rabi-dressed Feshbach resonances and hybrid bound states as a function of detuning δ/Ω . (a) Dressed scattering length for three sets of bare scattering lengths (a_{13}, a_{23}) corresponding to the points marked by $(\bullet, \blacklozenge, \blacksquare)$ symbols in Fig. 1(b). (b,c) Energy spectrum for $(a_{13}, a_{23})\sqrt{2m_r\Omega} = (-0.3, 0.8)$ in (b), and $(a_{13}, a_{23})\sqrt{2m_r\Omega} = (0.6, 0.8)$ in (c). We show the hybrid bound states (black lines), with the dashed red and blue lines corresponding to the bare 1-3 and 2-3 bound states. The purple lines show the dressed single-particle energies ϵ_{\pm} and the shaded area highlights the scattering continuum of the driven system.

be expressed as

$$\frac{1}{a_-} = \frac{1 - \sqrt{2m_r(\epsilon_+ - \epsilon_-)}(a_{13}s^2 + a_{23}c^2)}{a_{13}c^2 + a_{23}s^2 - a_{13}a_{23}\sqrt{2m_r(\epsilon_+ - \epsilon_-)}}, \quad (10a)$$

$$r_{\text{eff}} = \frac{-c^2s^2(a_{13} - a_{23})^2/\sqrt{2m_r(\epsilon_+ - \epsilon_-)}}{\left[a_{13}c^2 + a_{23}s^2 - a_{13}a_{23}\sqrt{2m_r(\epsilon_+ - \epsilon_-)} \right]^2}. \quad (10b)$$

In particular, we see that in general $a_- \neq a_{13}c^2 + a_{23}s^2$, and that the effective range $r_{\text{eff}} \leq 0$, similar to the case for a standard two-channel model of a magnetically tun-

able Feshbach resonance [40, 41]. We also note that when $a_{23} = 0$, Eq. (10a) reduces to the effective scattering length derived in Refs. [42, 43]. In the high-symmetry scenario where $a_{13} = a_{23} = a$, Eq. (10a) reduces to $a_- = a$, and thus for this special case, the dressed scattering length is independent of the Rabi drive and only diverges when a is itself divergent [44].

When $a_{13} \neq a_{23}$, however, a_- is strongly affected by the drive and can exhibit new resonances when the numerator of Eq. (10a) vanishes. Depending on the values of a_{13} and a_{23} , we find that this can occur for either zero, one, or two values of the dimensionless parameter δ/Ω . Figure 1(b) shows the existence diagram of the Rabi-induced resonances. The shaded areas are regions where resonances exist, while white denotes regions without a resonance. In the purple regions there exists a single resonance, whereas the gray area contains two resonances. To connect these regions, we note that on the horizontal (vertical) purple line boundary, a single resonance exists at negative (positive) detuning. When moving infinitesimally from the horizontal (vertical) axis into the gray area, a second resonance enters from $\delta \rightarrow \pm\infty$ and as we move further away from the axis along a vertical (horizontal) line, the second resonance approaches the initial resonance from above (below), and the two resonances eventually merge and vanish when Ω is sufficiently large (denoted by the black line).

Figure 3(a) shows the dressed scattering length and associated resonances, calculated for three sets of bare scattering lengths that are located in each colored area of the existence diagram, as indicated by the symbols (\bullet , \blacklozenge , \blacksquare) in Fig. 1(b). We see that the dressed scattering length exhibits a single resonance when only one of the bare scattering lengths is positive, while there are two resonances when both of the bare scattering lengths are positive, as expected from the existence diagram and the discussion above. One can also understand the behavior of a_- in the vicinity of the resonances, which we find can be approximated as

$$a_- \simeq a_{\text{bg}} \left(1 + \frac{\Gamma}{\delta - \delta_c} \right), \quad (11a)$$

$$\Gamma = \frac{1}{a_{\text{bg}}} \frac{c^2 s^2 (\epsilon_+ - \epsilon_-) (a_{13} - a_{23})^2}{2\sqrt{2m_r(\epsilon_+ - \epsilon_-)} + a_{13}s^2 - a_{23}c^2}, \quad (11b)$$

where we have introduced an effective background scattering length $a_{\text{bg}} = a_{13}c^2 + a_{23}s^2$, and ϵ_{\pm}, c, s are evaluated at the critical detuning δ_c . Hence, we expect the resonance width Γ to be reduced when $|a_{13} - a_{23}|$ decreases, as can be observed in Fig. 3(a), and to be enhanced when Ω increases. Interestingly, we see that Eq. (11a) resembles the typical two-channel behavior of a Feshbach resonance [1, 45, 46], although in the Rabi-driven case, a_{bg} also depends on the detuning. It also has the same form as the real part of the (inverse) effective scattering length in the presence of an oscillating magnetic field [47]. How-

ever, in our scenario the scattering length is purely real, and unlike the scenario in Ref. [47] the background scattering length itself depends on the applied field.

The scattering of the upper dressed state and an atom of species 3 is obtained in a similar manner, with $a_+ = (m_r/2\pi) [s^2 \mathbf{T}_{11}(\epsilon_+) + c^2 \mathbf{T}_{22}(\epsilon_+) + 2cs \mathbf{T}_{12}(\epsilon_+)]$. We obtain

$$\frac{1}{a_+} = \frac{1 + i\sqrt{2m_r(\epsilon_+ - \epsilon_-)}(a_{13}c^2 + a_{23}s^2)}{a_{13}s^2 + a_{23}c^2 + ia_{13}a_{23}\sqrt{2m_r(\epsilon_+ - \epsilon_-)}}. \quad (12)$$

In contrast to a_- , it does not exhibit any resonance and it is in general complex valued since the scattering takes place in the dressed continuum (except if $a_{13} = a_{23} = a$, in which case it reduces to $a_+ = a$). When $\sqrt{2m_r(\epsilon_+ - \epsilon_-)}(a_{13}c^2 + a_{23}s^2) \ll 1$, the effect of the continuum is less relevant and we have $a_+ \simeq (a_{13}s^2 + a_{23}c^2)$.

While we focus on fermions in this work, our few-body results apply to atoms of any statistics. Previous works have investigated the Feshbach resonances of rf-dressed bosonic atoms [35, 48–51] (see also Ref. [52]), but these typically involved scattering between identical bosons, unlike the scenario we consider where only one of the colliding particles is dressed. Furthermore, many proposals involve the coupling to a deeply bound molecular state, similar to the situation in an optical Feshbach resonance [53]. By contrast, our work uses a low-energy model featuring shallow bound states that can be strongly modified by the Rabi drive.

Hybrid bound states. — The origin of the dressed resonances can be understood through the two-body bound states of the Rabi-coupled system. The energy of these *hybrid* bound states can be calculated from the (real) poles of the T matrix (see the SM [38] for an equivalent solution starting from the Schrödinger equation).

Figure 3(b) illustrates the case where only one scattering length is positive. In this case, we find a single bound state below the continuum (shaded purple area starting at ϵ_-). At negative detuning the bound state approaches the bare bound state energy, $-1/(2m_r a_{23}^2) + \delta$, from below. On the other hand, when the hybrid bound state approaches the continuum at positive detuning, its energy is modified. The detuning at which the bound state enters the continuum corresponds to the position of a resonance in Fig. 3(a).

When a_{13} and a_{23} are both positive, we instead have two hybrid bound states, as shown in Fig. 3(c). In particular, we find that the upper and lower solutions involve 1-3 and 2-3 dimers that are either in or out of phase [38]. Away from the continuum, the bound-state energies interpolate between the bare bound states with a clear anticrossing, and they are well approximated by

$$\omega_{\pm} \simeq \frac{1}{2} \left(-\bar{\epsilon} + \delta \pm \sqrt{(\epsilon_{23} - \epsilon_{13} - \delta)^2 + \Omega^2} \right), \quad (13)$$

with $\bar{\epsilon} = \epsilon_{13} + \epsilon_{23}$ and $\epsilon_{ij} = 1/(2m_r a_{ij}^2)$. Here, ω_- corresponds to the ground state, which always exists, while

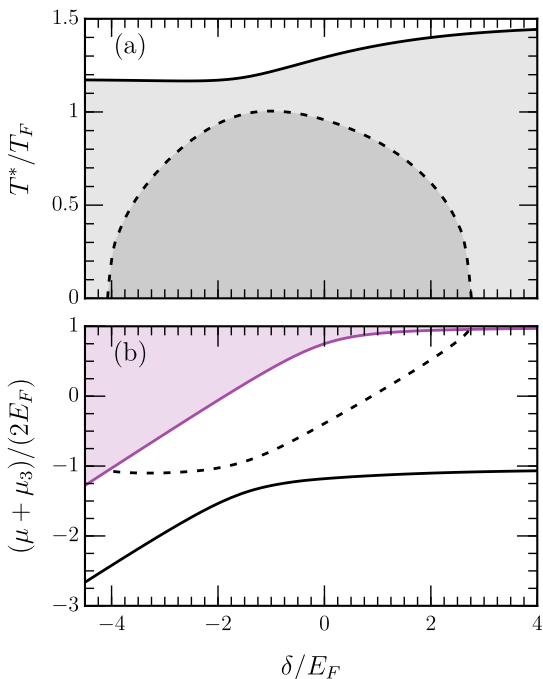


Figure 4. (a) Critical temperatures T^* for pairing at equal densities $n_1 + n_2 = n_3$, and (b) associated average chemical potentials versus detuning for $(a_{13}, a_{23})\sqrt{2m_r\Omega} = (0.6, 0.8)$, $\Omega/E_F = 1$ and equal masses $m_3 = m$. The black solid (dashed) lines correspond to ground (excited) state solutions. The purple line in (b) marks the edge of the dressed many-body continuum, given by $2E_F + \epsilon_-$.

ω_+ approximates the excited bound state and is only a true bound state outside of the continuum. Indeed, as we can see in Fig. 3(c), the excited bound state disappears when entering the continuum, and the two values of detunings at which this occurs correspond to the positions of resonances of a_- in Fig. 3(a). In the special case $a_{23} = a_{13} = a$, we find that Eq. (13) becomes exact with $\omega_{\pm} = \epsilon_{\pm} - 1/(2m_r a^2)$. Here, the excited hybrid bound state remains decoupled from the continuum of lower dressed particles, which explains the absence of a dressed Feshbach resonance mentioned above.

Pairing instabilities in a Rabi-coupled Fermi gas.— The results presented above have implications beyond two-body physics. Indeed, considering Fermi gases with a finite density, it is clear that the interactions allow for pairing to take place, which can give rise to a transition to a superfluid state. In conventional uncoupled Fermi systems, it is known that the pairing instability at finite temperature can be related to the many-body T matrix through the so-called Thouless criterion [36, 37]. We obtain a generalization of this criterion [54] for the Rabi-coupled system, which takes the form

$$\det[\mathbf{T}^{\text{mb}}(0)^{-1}] = 0, \quad (14)$$

where $\mathbf{T}^{\text{mb}}(\omega)$ denotes the many-body T matrix. It consists of the same diagrams as the two-body case [see Fig. 2(c)], adjusted to include the effect of Pauli exclusion due to the finite fermion density. Thus, \mathbf{T}^{mb} is given by Eq. (6) with $\mathbf{\Pi}$ replaced by its many-body counterpart, which accounts for this effect through the Fermi occupations of the dressed fermions $n_{\mathbf{q}\pm} = 1/(e^{\beta(\epsilon_{\mathbf{q}} + \epsilon_{\pm} - \mu)} + 1)$ and the third component $n_{\mathbf{q}3} = 1/(e^{\beta(\epsilon_{\mathbf{q}3} - \mu_3)} + 1)$, with the inverse temperature $\beta \equiv 1/T$ and chemical potentials μ and μ_3 describing the densities $n_1 + n_2$ and n_3 , respectively [38].

Solving Eq. (14) and the number equations self consistently allows us to determine the critical temperature for pairing (which is directly connected to the superfluid transition in the weak-coupling BCS regime) and the chemical potentials. Interestingly, we find that, similarly to the hybrid bound states in the two-body problem, there are regimes where two distinct pairing instabilities can occur, corresponding to 1-3 and 2-3 pairs that are either in phase or out of phase. The results of such a calculation for equal masses $m = m_3$ and balanced densities $n_1 + n_2 = n_3 \equiv k_F^3/6\pi^2$ are presented in Fig. 4, where we define the Fermi energy $E_F = k_F^2/2m$ and corresponding Fermi temperature $T_F = E_F$. We observe in Fig. 4(a) that a critical temperature always exists for the lowest energy many-body paired state (solid black line), and likewise there is a well-defined average chemical potential in Fig. 4(b). This suggests that the corresponding zero temperature ground state exhibits a superfluid *crossover* where the pairing evolves continuously from being dominated by the 2-3 channel at negative detuning to being dominated by 1-3 pairing at positive detuning. For the parameters chosen here where $a_{13}, a_{23} > 0$, this can be viewed as a BEC-BEC crossover, where the pseudospin of the pairs smoothly changes sign.

Additionally, Fig. 4(a) shows that there also exists an excited many-body paired state that vanishes at some critical detunings. This behavior is reflected in panel (b), which shows how the corresponding average chemical potentials reaches the Rabi-dressed many-body continuum at the same critical detunings. This signals that the excited state can undergo a transition from a superfluid to normal phase at these points. The excited-state superfluid can possibly be accessed dynamically by manipulating the bare scattering lengths such that the lower bound state is initially not present, i.e., by starting in the purple region in the vicinity of one of the purple lines in Fig. 1(b) and tuning across the purple line into the gray region with two resonances. As a function of detuning, this excited state experiences normal state-BCS transitions at the critical detunings where the chemical potential becomes that of two noninteracting Fermi seas, as well as a BCS-BEC-BCS crossover in between [54].

We stress that we have calculated the critical temperature using the number equations of fermions in the normal state, and thus, strictly speaking, it corresponds to

the critical temperature for fermion pairing to take place. While pairing is essential for the emergence of fermionic superfluids, it is well known that this criterion overestimates the transition temperature in the regime where the pairs are tightly bound, since it exceeds the condensation temperature of the ideal Bose gas of dimers [37, 55, 56]. This should be kept in mind for the interpretation of the large values of T^* obtained in Fig. 4. Nonetheless, our results clearly illustrate that one can tune across the entire BCS-BEC crossover by varying the parameters of the Rabi drive alone.

Finally, we comment on the stability of the Rabi-coupled Fermi gas. In general, strongly interacting three-component Fermi gases are unstable towards three-body recombination [12, 30]. While this is not an issue for the two-body physics described above, as it only involves two particles, the Rabi-dressed many-body system necessarily features all three bare fermionic components. However, we note that, in our setup, the absence of 1-2 interactions strongly suppresses both Efimov physics and three-body losses compared with the case where all components interact near resonantly [57]. Additional stability can be achieved by considering $\Omega \gtrsim E_F, T$ such that the population of the upper dressed state remains small and we are left with an effective two-component Fermi gas. Indeed, the polaron limit of the strongly Rabi-driven Fermi gas was investigated in Ref. [29], and despite the significant impurity fraction of 1:5 the authors did not find that losses noticeably impacted their measurements.

Conclusions. — We have shown that the presence of a Rabi drive can strongly modify the interactions in ultracold atomic gases. Using a T -matrix calculation, we have demonstrated that the scattering between a Rabi-driven and an undriven atom can exhibit resonances, which arise when hybrid bound states enter the Rabi-dressed scattering continuum. Beyond the two-body physics, we find that these results have implications for the pairing instabilities in the Rabi-coupled Fermi gas. Specifically, we have shown that for a given set of bare scattering lengths, one can use the detuning to control the transition temperature and tune the system across superfluid crossovers. We expect that our findings will be relevant for other few and many body phenomena in Rabi-coupled mixtures, such as Efimov states [43] or ground-state transitions in spin-imbalanced gases [58–60]. The investigation of these mixtures may also shed light on other physical systems difficult to access experimentally. For example, the three-component Fermi gas is known to have connections with quark matter [61–64], and similar analogies may exist in the Rabi-driven case [65]. Furthermore, it could provide a useful analog of light-driven materials, allowing one to simulate phenomena such as light-enhanced superconductivity [66, 67].

We gratefully acknowledge fruitful discussions with Henning Moritz, Nir Navon, and Anthony Zulli. OB, BCM, JL, and MMP acknowledge support from the

Australian Research Council (ARC) Centre of Excellence in Future Low-Energy Electronics Technologies (CE170100039), and from ARC Discovery Projects DP240100569 and DP250103746. MMP is also supported through an ARC Future Fellowship FT200100619. CRC is supported by the Cluster of Excellence “CUI: Advanced Imaging of Matter”—EXC 2056—project ID 390715994.

* These two authors contributed equally to this work.

- [1] C. Chin, R. Grimm, P. Julienne, and E. Tiesinga, *Feshbach resonances in ultracold gases*, *Rev. Mod. Phys.* **82**, 1225 (2010).
- [2] I. Bloch, J. Dalibard, and S. Nascimbène, *Quantum simulations with ultracold quantum gases*, *Nature Physics* **8**, 267 (2012).
- [3] C. A. Regal, M. Greiner, and D. S. Jin, *Observation of Resonance Condensation of Fermionic Atom Pairs*, *Phys. Rev. Lett.* **92**, 040403 (2004).
- [4] M. W. Zwierlein, C. A. Stan, C. H. Schunck, S. M. F. Raupach, A. J. Kerman, and W. Ketterle, *Condensation of Pairs of Fermionic Atoms near a Feshbach Resonance*, *Phys. Rev. Lett.* **92**, 120403 (2004).
- [5] T. Bourdel, L. Khaykovich, J. Cubizolles, J. Zhang, F. Chevy, M. Teichmann, L. Tarruell, S. J. J. M. F. Kokkelmans, and C. Salomon, *Experimental Study of the BEC-BCS Crossover Region in Lithium 6*, *Phys. Rev. Lett.* **93**, 050401 (2004).
- [6] C. Chin, M. Bartenstein, A. Altmeyer, S. Riedl, S. Jochim, J. H. Denschlag, and R. Grimm, *Observation of the Pairing Gap in a Strongly Interacting Fermi Gas*, *Science* **305**, 1128 (2004).
- [7] A. Schirotzek, C.-H. Wu, A. Sommer, and M. W. Zwierlein, *Observation of Fermi Polarons in a Tunable Fermi Liquid of Ultracold Atoms*, *Phys. Rev. Lett.* **102**, 230402 (2009).
- [8] S. Nascimbène, N. Navon, K. J. Jiang, L. Tarruell, M. Teichmann, J. McKeever, F. Chevy, and C. Salomon, *Collective Oscillations of an Imbalanced Fermi Gas: Axial Compression Modes and Polaron Effective Mass*, *Phys. Rev. Lett.* **103**, 170402 (2009).
- [9] M.-G. Hu, M. J. Van de Graaff, D. Kedar, J. P. Corson, E. A. Cornell, and D. S. Jin, *Bose Polarons in the Strongly Interacting Regime*, *Phys. Rev. Lett.* **117**, 055301 (2016).
- [10] N. B. Jørgensen, L. Wacker, K. T. Skalmstang, M. M. Parish, J. Levinsen, R. S. Christensen, G. M. Bruun, and J. J. Arlt, *Observation of Attractive and Repulsive Polarons in a Bose-Einstein Condensate*, *Phys. Rev. Lett.* **117**, 055302 (2016).
- [11] T. Kraemer, M. Mark, P. Waldburger, J. G. Danzl, C. Chin, B. Engeser, A. D. Lange, K. Pilch, A. Jaakkola, H.-C. Nägerl, and R. Grimm, *Evidence for Efimov quantum states in an ultracold gas of caesium atoms*, *Nature* **440**, 315 (2006).
- [12] T. Lompe, T. B. Ottenstein, F. Serwane, A. N. Wenz, G. Zürn, and S. Jochim, *Radio-Frequency Association of Efimov Trimers*, *Science* **330**, 940 (2010).

- [13] M. Punk and W. Zwerger, *Theory of rf-Spectroscopy of Strongly Interacting Fermions*, *Phys. Rev. Lett.* **99**, 170404 (2007).
- [14] M. Cetina, M. Jag, R. S. Lous, I. Fritsche, J. T. M. Walraven, R. Grimm, J. Levinsen, M. M. Parish, R. Schmidt, M. Knap, and E. Demler, *Ultrafast many-body interferometry of impurities coupled to a Fermi sea*, *Science* **354**, 96 (2016).
- [15] C. J. Vale and M. Zwierlein, *Spectroscopic probes of quantum gases*, *Nature Physics* **17**, 1305 (2021).
- [16] M. R. Matthews, B. P. Anderson, P. C. Haljan, D. S. Hall, M. J. Holland, J. E. Williams, C. E. Wieman, and E. A. Cornell, *Watching a Superfluid Untwist Itself: Recurrence of Rabi Oscillations in a Bose-Einstein Condensate*, *Phys. Rev. Lett.* **83**, 3358 (1999).
- [17] C. Kohstall, M. Zaccanti, M. Jag, A. Trenkwalder, P. Massignan, G. M. Bruun, F. Schreck, and R. Grimm, *Metastability and coherence of repulsive polarons in a strongly interacting Fermi mixture*, *Nature* **485**, 615 (2012).
- [18] M. Koschorreck, D. Pertot, E. Vogt, B. Fröhlich, M. Feld, and M. Köhl, *Attractive and repulsive Fermi polarons in two dimensions*, *Nature* **485**, 619 (2012).
- [19] F. Scazza, G. Valtolina, P. Massignan, A. Recati, A. Amico, A. Burchianti, C. Fort, M. Inguscio, M. Zaccanti, and G. Roati, *Repulsive Fermi Polarons in a Resonant Mixture of Ultracold ^6Li Atoms*, *Phys. Rev. Lett.* **118**, 083602 (2017).
- [20] N. Darkwah Oppong, L. Riegger, O. Bettermann, M. Höfer, J. Levinsen, M. M. Parish, I. Bloch, and S. Fölling, *Observation of Coherent Multiorbital Polarons in a Two-Dimensional Fermi Gas*, *Phys. Rev. Lett.* **122**, 193604 (2019).
- [21] H. S. Adlong, W. E. Liu, F. Scazza, M. Zaccanti, N. D. Oppong, S. Fölling, M. M. Parish, and J. Levinsen, *Quasiparticle Lifetime of the Repulsive Fermi Polaron*, *Phys. Rev. Lett.* **125**, 133401 (2020).
- [22] T. Zibold, E. Nicklas, C. Gross, and M. K. Oberthaler, *Classical Bifurcation at the Transition from Rabi to Josephson Dynamics*, *Phys. Rev. Lett.* **105**, 204101 (2010).
- [23] E. Nicklas, H. Strobel, T. Zibold, C. Gross, B. A. Malomed, P. G. Kevrekidis, and M. K. Oberthaler, *Rabi Flopping Induces Spatial Demixing Dynamics*, *Phys. Rev. Lett.* **107**, 193001 (2011).
- [24] L. Lavoine, A. Hammond, A. Recati, D. S. Petrov, and T. Bourdel, *Beyond-Mean-Field Effects in Rabi-Coupled Two-Component Bose-Einstein Condensate*, *Phys. Rev. Lett.* **127**, 203402 (2021).
- [25] A. Hammond, L. Lavoine, and T. Bourdel, *Tunable Three-Body Interactions in Driven Two-Component Bose-Einstein Condensates*, *Phys. Rev. Lett.* **128**, 083401 (2022).
- [26] J. Sanz, A. Frölian, C. S. Chisholm, C. R. Cabrera, and L. Tarruell, *Interaction Control and Bright Solitons in Coherently Coupled Bose-Einstein Condensates*, *Phys. Rev. Lett.* **128**, 013201 (2022).
- [27] R. Cominotti, A. Berti, C. Dulin, C. Rogora, G. Lamporesi, I. Carusotto, A. Recati, A. Zenesini, and G. Ferrari, *Ferromagnetism in an Extended Coherently Coupled Atomic Superfluid*, *Phys. Rev. X* **13**, 021037 (2023).
- [28] A. Zenesini, A. Berti, R. Cominotti, C. Rogora, I. G. Moss, T. P. Billam, I. Carusotto, G. Lamporesi, A. Recati, and G. Ferrari, *False vacuum decay via bubble formation in ferromagnetic superfluids*, *Nature Physics* **20**, 558 (2024).
- [29] F. J. Vivanco, A. Schuckert, S. Huang, G. L. Schumacher, G. G. T. Assumpção, Y. Ji, J. Chen, M. Knap, and N. Navon, *The strongly driven Fermi polaron*, [arXiv:2308.05746](https://arxiv.org/abs/2308.05746) (2023).
- [30] T. B. Ottenstein, T. Lompe, M. Kohnen, A. N. Wenz, and S. Jochim, *Collisional Stability of a Three-Component Degenerate Fermi Gas*, *Phys. Rev. Lett.* **101**, 203202 (2008).
- [31] J. H. Huckans, J. R. Williams, E. L. Hazlett, R. W. Stites, and K. M. O'Hara, *Three-Body Recombination in a Three-State Fermi Gas with Widely Tunable Interactions*, *Phys. Rev. Lett.* **102**, 165302 (2009).
- [32] J. R. Williams, E. L. Hazlett, J. H. Huckans, R. W. Stites, Y. Zhang, and K. M. O'Hara, *Evidence for an Excited-State Efimov Trimer in a Three-Component Fermi Gas*, *Phys. Rev. Lett.* **103**, 130404 (2009).
- [33] G. L. Schumacher, J. T. Mäkinen, Y. Ji, G. G. T. Assumpção, J. Chen, S. Huang, F. J. Vivanco, and N. Navon, *Observation of Anomalous Decay of a Polarized Three-Component Fermi Gas* (2023), [arXiv:2301.02237](https://arxiv.org/abs/2301.02237) [cond-mat.quant-gas].
- [34] P. Zhang, P. Naidon, and M. Ueda, *Independent Control of Scattering Lengths in Multicomponent Quantum Gases*, *Phys. Rev. Lett.* **103**, 133202 (2009).
- [35] T. M. Hanna, E. Tiesinga, and P. S. Julienne, *Creation and manipulation of Feshbach resonances with radiofrequency radiation*, *New Journal of Physics* **12**, 083031 (2010).
- [36] D. J. Thouless, *Perturbation theory in statistical mechanics and the theory of superconductivity*, *Annals of Physics* **10**, 553 (1960).
- [37] G. C. Strinati, P. Pieri, G. Röpke, P. Schuck, and M. Urban, *The BCS-BEC crossover: From ultra-cold Fermi gases to nuclear systems*, *Physics Reports* **738**, 1 (2018).
- [38] See the Supplemental Material for details on the T -matrix calculation, and the derivation of the hybrid bound states using the Schrödinger equation. The Supplemental Material includes reference to [68, 69].
- [39] C. P. Search and P. R. Berman, *Manipulating the speed of sound in a two-component Bose-Einstein condensate*, *Phys. Rev. A* **63**, 043612 (2001).
- [40] E. Timmermans, P. Tommasini, M. Hussein, and A. Kerman, *Feshbach resonances in atomic Bose-Einstein condensates*, *Physics Reports* **315**, 199 (1999).
- [41] V. Gurarie and L. Radzihovsky, *Resonantly paired fermionic superfluids*, *Annals of Physics* **322**, 2 (2007).
- [42] B. C. Mulkerin, J. Levinsen, and M. M. Parish, *Rabi oscillations and magnetization of a mobile spin-1/2 impurity in a Fermi sea*, *Phys. Rev. A* **109**, 023302 (2024).
- [43] A. N. Zulli, B. C. Mulkerin, M. M. Parish, and J. Levinsen, *Universal Efimov Scaling in the Rabi-Coupled Few-Body Spectrum* (2025), [arXiv:2501.18844](https://arxiv.org/abs/2501.18844).
- [44] Indeed, when $a_{13} = a_{23} = a$, the T matrix reduces to that in the absence of Rabi coupling, independent of the parameters of the Rabi drive, with $T_{-}(\epsilon_{-} + \epsilon_{\mathbf{k}} + \epsilon_{\mathbf{k}3}) = \frac{2\pi}{m_r} \frac{1}{a^{-1} + ik}$.
- [45] A. J. Moerdijk, B. J. Verhaar, and A. Axelsson, *Resonances in ultracold collisions of ^6Li , ^7Li , and ^{23}Na* , *Phys. Rev. A* **51**, 4852 (1995).
- [46] S. Inouye, M. R. Andrews, J. Stenger, H.-J. Miesner, D. M. Stamper-Kurn, and W. Ketterle, *Observation of*

- Feshbach resonances in a Bose-Einstein condensate*, *Nature* **392**, 151 (1998).
- [47] D. H. Smith, *Inducing Resonant Interactions in Ultracold Atoms with a Modulated Magnetic Field*, *Phys. Rev. Lett.* **115**, 193002 (2015).
- [48] A. J. Moerdijk, B. J. Verhaar, and T. M. Nagtegaal, *Collisions of dressed ground-state atoms*, *Phys. Rev. A* **53**, 4343 (1996).
- [49] A. M. Kaufman, R. P. Anderson, T. M. Hanna, E. Tiesinga, P. S. Julienne, and D. S. Hall, *Radio-frequency dressing of multiple Feshbach resonances*, *Phys. Rev. A* **80**, 050701 (2009).
- [50] T. V. Tscherbul, T. Calarco, I. Lesanovsky, R. V. Krems, A. Dalgarno, and J. Schmiedmayer, *rf-field-induced Feshbach resonances*, *Phys. Rev. A* **81**, 050701 (2010).
- [51] D. J. Papoular, G. V. Shlyapnikov, and J. Dalibard, *Microwave-induced Fano-Feshbach resonances*, *Phys. Rev. A* **81**, 041603 (2010).
- [52] D. S. Petrov, *Three-Body Interacting Bosons in Free Space*, *Phys. Rev. Lett.* **112**, 103201 (2014).
- [53] P. O. Fedichev, Y. Kagan, G. V. Shlyapnikov, and J. T. M. Walraven, *Influence of Nearly Resonant Light on the Scattering Length in Low-Temperature Atomic Gases*, *Phys. Rev. Lett.* **77**, 2913 (1996).
- [54] B. C. Mulkerin, O. Bleu, C. R. Cabrera, J. Levinsen, and M. M. Parish, in preparation.
- [55] P. Nozières and S. Schmitt-Rink, *Bose condensation in an attractive fermion gas: From weak to strong coupling superconductivity*, *Journal of Low Temperature Physics* **59**, 195 (1985).
- [56] C. A. R. Sá de Melo, M. Randeria, and J. R. Engelbrecht, *Crossover from BCS to Bose superconductivity: Transition temperature and time-dependent Ginzburg-Landau theory*, *Phys. Rev. Lett.* **71**, 3202 (1993).
- [57] E. Braaten and H.-W. Hammer, *Universality in few-body systems with large scattering length*, *Physics Reports* **428**, 259 (2006).
- [58] C. Mora and F. Chevy, *Ground state of a tightly bound composite dimer immersed in a Fermi sea*, *Phys. Rev. A* **80**, 033607 (2009).
- [59] M. Punk, P. T. Dumitrescu, and W. Zwerger, *Polaron-to-molecule transition in a strongly imbalanced Fermi gas*, *Phys. Rev. A* **80**, 053605 (2009).
- [60] R. Combescot, S. Giraud, and X. Leyronas, *Analytical theory of the dressed bound state in highly polarized Fermi gases*, *Europhysics Letters* **88**, 60007 (2010).
- [61] A. Rapp, G. Zaránd, C. Honerkamp, and W. Hofstetter, *Color Superfluidity and “Baryon” Formation in Ultracold Fermions*, *Phys. Rev. Lett.* **98**, 160405 (2007).
- [62] F. Wilczek, *Lifestyles of the small and simple*, *Nature Physics* **3**, 375 (2007).
- [63] T. Ozawa and G. Baym, *Population imbalance and pairing in the BCS-BEC crossover of three-component ultracold fermions*, *Phys. Rev. A* **82**, 063615 (2010).
- [64] K. M. O’Hara, *Realizing analogues of color superconductivity with ultracold alkali atoms*, *New Journal of Physics* **13**, 065011 (2011).
- [65] D. M. Kurcuoglu and C. A. R. Sá de Melo, *Color superfluidity of neutral ultracold fermions in the presence of color-flip and color-orbit fields*, *Phys. Rev. A* **97**, 023632 (2018).
- [66] D. Fausti, R. I. Tobey, N. Dean, S. Kaiser, A. Dienst, M. C. Hoffmann, S. Pyon, T. Takayama, H. Takagi, and A. Cavalleri, *Light-Induced Superconductivity in a Stripe-Ordered Cuprate*, *Science* **331**, 189 (2011).
- [67] M. Mitrano, A. Cantaluppi, D. Nicoletti, S. Kaiser, A. Perucchi, S. Lupi, P. Di Pietro, D. Pontiroli, M. Riccò, S. R. Clark, D. Jaksch, and A. Cavalleri, *Possible light-induced superconductivity in K_3C_{60} at high temperature*, *Nature* **530**, 461 (2016).
- [68] G. Li, O. Bleu, J. Levinsen, and M. M. Parish, *Theory of polariton-electron interactions in semiconductor microcavities*, *Phys. Rev. B* **103**, 195307 (2021).
- [69] H. Hu and X.-J. Liu, *Fermi spin polaron and dissipative Fermi-polaron Rabi dynamics*, *Phys. Rev. A* **108**, 063312 (2023).

SUPPLEMENTAL MATERIAL: Scattering resonances and pairing in a Rabi-coupled Fermi gas

Olivier Bleu,¹ Brendan C. Mulkerin,¹ Cesar R. Cabrera,^{2,3} Jesper Levinsen,¹ Meera M. Parish¹

¹*School of Physics and Astronomy, Monash University, Victoria 3800, Australia*

²*Institute for Quantum Physics, Universität Hamburg, Luruper Chaussee 149, 22761 Hamburg, Germany*

³*The Hamburg Centre for Ultrafast Imaging, Universität Hamburg, Luruper Chaussee 149, 22761 Hamburg, Germany*

Details on the calculation of the T matrix

In this section, we provide additional details on the calculation of the T matrix. As shown in the main text, the two-body T matrix is of the form

$$\mathbf{T}(\omega) = [\mathbf{g}^{-1} - \mathbf{\Pi}(\omega)]^{-1}, \quad (\text{S1})$$

with

$$\Pi_{\sigma\sigma'}(\omega) = \int \frac{d\omega'}{2i\pi} \sum_{\mathbf{q}} G_{\sigma\sigma'}(-\mathbf{q}, -\omega') G_3(\mathbf{q}, \omega + \omega'). \quad (\text{S2})$$

The non-interacting Green's function of the third species is given by $G_3(\mathbf{k}, \omega) = (\omega - \epsilon_{\mathbf{k}3} + i0)^{-1}$, and those of the Rabi-coupled species $G_{\sigma\sigma'}(\mathbf{k}, \omega) = \langle 0 | \hat{f}_{\mathbf{k}\sigma'}(\omega - \hat{H}_0 + i0)^{-1} \hat{f}_{\mathbf{k}\sigma}^\dagger | 0 \rangle$ read [42, 69]

$$G_{11}(\mathbf{k}, \omega) = \frac{c^2}{\omega - \epsilon_{\mathbf{k}} - \epsilon_-} + \frac{s^2}{\omega - \epsilon_{\mathbf{k}} - \epsilon_+}, \quad (\text{S3a})$$

$$G_{22}(\mathbf{k}, \omega) = \frac{s^2}{\omega - \epsilon_{\mathbf{k}} - \epsilon_-} + \frac{c^2}{\omega - \epsilon_{\mathbf{k}} - \epsilon_+}, \quad (\text{S3b})$$

$$G_{12}(\mathbf{k}, \omega) = G_{21}(\mathbf{k}, \omega) = \frac{-cs}{\omega - \epsilon_{\mathbf{k}} - \epsilon_-} + \frac{cs}{\omega - \epsilon_{\mathbf{k}} - \epsilon_+}. \quad (\text{S3c})$$

This allows us to evaluate the frequency integrals in the pair functions $\Pi_{\sigma\sigma'}$, which gives

$$\Pi_{11}(\omega) = \sum_{\mathbf{q}} \left[\frac{c^2}{\omega - \bar{\epsilon}_{\mathbf{q}} - \epsilon_-} + \frac{s^2}{\omega - \bar{\epsilon}_{\mathbf{q}} - \epsilon_+} \right], \quad (\text{S4a})$$

$$\Pi_{22}(\omega) = \sum_{\mathbf{q}} \left[\frac{s^2}{\omega - \bar{\epsilon}_{\mathbf{q}} - \epsilon_-} + \frac{c^2}{\omega - \bar{\epsilon}_{\mathbf{q}} - \epsilon_+} \right], \quad (\text{S4b})$$

$$\Pi_{12}(\omega) = \Pi_{21}(\omega) = \sum_{\mathbf{q}} \left[\frac{-cs}{\omega - \bar{\epsilon}_{\mathbf{q}} - \epsilon_-} + \frac{cs}{\omega - \bar{\epsilon}_{\mathbf{q}} - \epsilon_+} \right], \quad (\text{S4c})$$

where we have introduced $\bar{\epsilon}_{\mathbf{q}} = \epsilon_{\mathbf{q}3} + \epsilon_{\mathbf{q}}$. The momentum integrals can then be evaluated analytically, and the elements of the inverse T matrix read

$$\frac{1}{g_{13}} - \Pi_{11}(\omega) = \frac{m_r}{2\pi} \left[\frac{1}{a_{13}} - \left(c^2 \sqrt{2m_r(\epsilon_- - \omega)} + s^2 \sqrt{2m_r(\epsilon_+ - \omega)} \right) \right], \quad (\text{S5a})$$

$$\frac{1}{g_{23}} - \Pi_{22}(\omega) = \frac{m_r}{2\pi} \left[\frac{1}{a_{23}} - \left(s^2 \sqrt{2m_r(\epsilon_- - \omega)} + c^2 \sqrt{2m_r(\epsilon_+ - \omega)} \right) \right], \quad (\text{S5b})$$

$$\Pi_{12}(\omega) = \Pi_{21}(\omega) = cs \frac{m_r}{2\pi} \left[-\sqrt{2m_r(\epsilon_- - \omega)} + \sqrt{2m_r(\epsilon_+ - \omega)} \right]. \quad (\text{S5c})$$

Many-body T matrix

The many-body T matrix of the Rabi coupled Fermi gas has the same form as the two-body T matrix but with $\mathbf{\Pi}$ replaced by its many-body version $\mathbf{\Pi}^{\text{mb}}$ which accounts for the Pauli blocking of identical fermions.

$$\mathbf{T}^{\text{mb}}(\omega) = [\mathbf{g}^{-1} - \mathbf{\Pi}^{\text{mb}}(\omega)]^{-1}. \quad (\text{S6})$$

Specifically, the elements of $\mathbf{\Pi}^{\text{mb}}$ are given by

$$\Pi_{11}^{\text{mb}}(\omega) = \sum_{\mathbf{q}} \left[\frac{c^2(1 - n_{\mathbf{q}3} - n_{\mathbf{q}-})}{\omega - \bar{\xi}_{\mathbf{q}} - \epsilon_-} + \frac{s^2(1 - n_{\mathbf{q}3} - n_{\mathbf{q}+})}{\omega - \bar{\xi}_{\mathbf{q}} - \epsilon_+} \right], \quad (\text{S7a})$$

$$\Pi_{22}^{\text{mb}}(\omega) = \sum_{\mathbf{q}} \left[\frac{s^2(1 - n_{\mathbf{q}3} - n_{\mathbf{q}-})}{\omega - \bar{\xi}_{\mathbf{q}} - \epsilon_-} + \frac{c^2(1 - n_{\mathbf{q}3} - n_{\mathbf{q}+})}{\omega - \bar{\xi}_{\mathbf{q}} - \epsilon_+} \right], \quad (\text{S7b})$$

$$\Pi_{12}^{\text{mb}}(\omega) = \Pi_{21}^{\text{mb}}(\omega) = \sum_{\mathbf{q}} \left[\frac{-cs(1 - n_{\mathbf{q}3} - n_{\mathbf{q}-})}{\omega - \bar{\xi}_{\mathbf{q}} - \epsilon_-} + \frac{cs(1 - n_{\mathbf{q}3} - n_{\mathbf{q}+})}{\omega - \bar{\xi}_{\mathbf{q}} - \epsilon_+} \right]. \quad (\text{S7c})$$

Here, we have introduced the Fermi occupations of the Rabi-dressed fermions $n_{\mathbf{q}\pm} = 1/(e^{\beta(\epsilon_{\mathbf{q}} + \epsilon_{\pm} - \mu)} + 1)$ and of the third component $n_{\mathbf{q}3} = 1/(e^{\beta(\epsilon_{\mathbf{q}3} - \mu_3)} + 1)$ with the chemical potentials μ and μ_3 . We have also defined $\bar{\xi}_{\mathbf{q}} = \epsilon_{\mathbf{q}} - \mu + \epsilon_{\mathbf{q}3} - \mu_3$.

The associated number equations for the densities n_1 , n_2 and n_3 of the three components in the many-body system are:

$$n_1 + n_2 = \sum_{\mathbf{q}} \left(\frac{1}{e^{\beta(\epsilon_{\mathbf{q}} + \epsilon_+ - \mu)} + 1} + \frac{1}{e^{\beta(\epsilon_{\mathbf{q}} + \epsilon_- - \mu)} + 1} \right), \quad (\text{S8})$$

$$n_3 = \sum_{\mathbf{q}} \frac{1}{e^{\beta(\epsilon_{\mathbf{q}3} - \mu_3)} + 1}. \quad (\text{S9})$$

We use these number equations to calculate the pairing instability temperatures and the chemical potentials at a fixed density as shown in Fig. 4 of the main text.

Bound states using the Schrödinger equation

Alternatively, we can obtain the two-body bound states by solving the Schrödinger equation. This allows us to show that the bound-state energy can be obtained from the poles of the dressed T matrix, as done in the main text, and, in addition, to derive the corresponding wave functions.

We are interested in calculating the two-body bound states between a dressed particle (superposition of species 1 and 2) and a particle from species 3. The most general two-body wave function takes the form

$$|\psi\rangle = \sum_{\mathbf{k}} \varphi_{\mathbf{k}} \hat{f}_{\mathbf{k}3}^{\dagger} \left(c_{\mathbf{k}} \hat{f}_{-\mathbf{k}1}^{\dagger} + s_{\mathbf{k}} \hat{f}_{-\mathbf{k}2}^{\dagger} \right) |0\rangle. \quad (\text{S10})$$

Note that $c_{\mathbf{k}}$ and $s_{\mathbf{k}}$ are part of the bound state wave function that we wish to determine and differ from the single-particle mixing coefficients. Projecting the two-body Schrödinger equation $\hat{H}|\psi\rangle = E|\psi\rangle$ onto its components, we obtain

$$(E - \bar{\epsilon}_{\mathbf{k}}) \varphi_{\mathbf{k}} c_{\mathbf{k}} - \frac{\Omega}{2} \varphi_{\mathbf{k}} s_{\mathbf{k}} = g_{13} \sum_{\mathbf{q}} \varphi_{\mathbf{q}} c_{\mathbf{q}}, \quad (\text{S11a})$$

$$(E - \bar{\epsilon}_{\mathbf{k}} - \delta) \varphi_{\mathbf{k}} s_{\mathbf{k}} - \frac{\Omega}{2} \varphi_{\mathbf{k}} c_{\mathbf{k}} = g_{23} \sum_{\mathbf{q}} \varphi_{\mathbf{q}} s_{\mathbf{q}}. \quad (\text{S11b})$$

Taking the ratio of the two parts in Eq. (S11) we obtain an equation for $t_{\mathbf{k}} = s_{\mathbf{k}}/c_{\mathbf{k}}$

$$t_{\mathbf{k}} = \frac{\Omega + 2(E - \bar{\epsilon}_{\mathbf{k}})R}{2(E - \bar{\epsilon}_{\mathbf{k}} - \delta) + \Omega R}, \quad (\text{S12})$$

where we have introduced the parameter R

$$R = \frac{g_{23} \sum_{\mathbf{q}} \varphi_{\mathbf{q}} s_{\mathbf{q}}}{g_{13} \sum_{\mathbf{q}} \varphi_{\mathbf{q}} c_{\mathbf{q}}}.$$

Multiplying (S11a) by g_{13} and (S11b) by g_{23} , dividing both sides by $(E - \dots)$ and summing over \mathbf{k} , these equations can be rearranged as

$$\frac{1}{g_{13}} = \sum_{\mathbf{k}} \frac{1}{E - \bar{\epsilon}_{\mathbf{k}} - \frac{\Omega}{2}t_{\mathbf{k}}}, \quad (\text{S13a})$$

$$\frac{1}{g_{23}} = \sum_{\mathbf{k}} \frac{1}{E - \bar{\epsilon}_{\mathbf{k}} - \delta - \frac{\Omega}{2}t_{\mathbf{k}}}. \quad (\text{S13b})$$

Using Eq. (S12), we obtain

$$\frac{1}{g_{13}} = \sum_{\mathbf{k}} \frac{E - \bar{\epsilon}_{\mathbf{k}} - \delta + \frac{\Omega}{2}R}{(E - \bar{\epsilon}_{\mathbf{k}})(E - \bar{\epsilon}_{\mathbf{k}} - \delta) - \frac{\Omega^2}{4}}, \quad (\text{S14a})$$

$$\frac{1}{g_{23}} = \sum_{\mathbf{k}} \frac{E - \bar{\epsilon}_{\mathbf{k}} + \frac{\Omega}{2}R}{(E - \bar{\epsilon}_{\mathbf{k}})(E - \bar{\epsilon}_{\mathbf{k}} - \delta) - \frac{\Omega^2}{4}}. \quad (\text{S14b})$$

Here we can recognize

$$\frac{1}{g_{13}} = \Pi_{11}(E) + R\Pi_{12}(E), \quad (\text{S15a})$$

$$\frac{1}{g_{23}} = \Pi_{22}(E) + \Pi_{21}(E)/R, \quad (\text{S15b})$$

with the functions Π_{ij} defined in Eq. (S4). Isolating R in the first line and injecting it in the second we obtain

$$\det[\mathbf{g}^{-1} - \mathbf{\Pi}(E)] = 0, \quad (\text{S16})$$

which corresponds to the equation for the poles of the dressed T matrix (6).

The solutions of (S16) correspond to bound states with energy $E = \epsilon_- - \varepsilon$ (where the binding energy $\varepsilon > 0$ is measured from ϵ_-). One can then use (S15) to determine R

$$\begin{aligned} R(\varepsilon) &= \frac{\frac{1}{g_{13}} - \Pi_{11}(\epsilon_- - \varepsilon)}{\Pi_{12}(\epsilon_- - \varepsilon)}, \quad (\text{S17}) \\ &= \frac{\frac{1}{a_{13}} - \left(c^2 \sqrt{2m_r \varepsilon} + s^2 \sqrt{2m_r(\varepsilon + \epsilon_+ - \epsilon_-)} \right)}{cs \left(\sqrt{2m_r(\varepsilon + \epsilon_+ - \epsilon_-)} - \sqrt{2m_r \varepsilon} \right)}. \end{aligned}$$

We can also find the wave function of the bound state in a manner analogous to that used in Ref. [68]. Since the right hand side of the Schrödinger equation (S11) is independent of momentum, we must have

$$\begin{aligned} \varphi_{\mathbf{k}c\mathbf{k}} &= \frac{\mathcal{C}}{\varepsilon - \epsilon_- + \bar{\epsilon}_{\mathbf{k}} + \frac{\Omega}{2}t_{\mathbf{k}}} \\ &= \mathcal{C} \left(\frac{c^2 - csR}{\varepsilon + \bar{\epsilon}_{\mathbf{k}}} + \frac{s^2 + csR}{\varepsilon + \epsilon_+ - \epsilon_- + \bar{\epsilon}_{\mathbf{k}}} \right), \quad (\text{S18a}) \end{aligned}$$

$$\begin{aligned} \varphi_{\mathbf{k}s\mathbf{k}} &= \frac{\mathcal{S}}{\varepsilon - \epsilon_- + \bar{\epsilon}_{\mathbf{k}} + \delta + \frac{\Omega}{2}t_{\mathbf{k}}} \\ &= \mathcal{S} \left(\frac{s^2 - cs/R}{\varepsilon + \bar{\epsilon}_{\mathbf{k}}} + \frac{c^2 + cs/R}{\varepsilon + \epsilon_+ - \epsilon_- + \bar{\epsilon}_{\mathbf{k}}} \right), \quad (\text{S18b}) \end{aligned}$$

where the coefficients \mathcal{C} and \mathcal{S} are determined by the normalization condition of the wave function and Eq. (S12). From (S12), we have the relation $\mathcal{S}/\mathcal{C} = R$, with the sign of R determined by Eq. (S17), while the normalization imposes

$$\begin{aligned} \frac{1}{\mathcal{C}^2} &= \sum_{\mathbf{k}} \frac{1}{(\varepsilon - \epsilon_- + \bar{\epsilon}_{\mathbf{k}} + \frac{\Omega}{2}t_{\mathbf{k}})^2} + \frac{R^2}{(\varepsilon - \epsilon_- + \bar{\epsilon}_{\mathbf{k}} + \delta + \frac{\Omega}{2}t_{\mathbf{k}})^2} \\ &= \frac{m_r^{3/2}}{2\sqrt{2}\pi} \left[\frac{(cR + s)^2}{\sqrt{\varepsilon + \epsilon_+ - \epsilon_-}} + \frac{(sR - c)^2}{\sqrt{\varepsilon}} \right]. \quad (\text{S19}) \end{aligned}$$

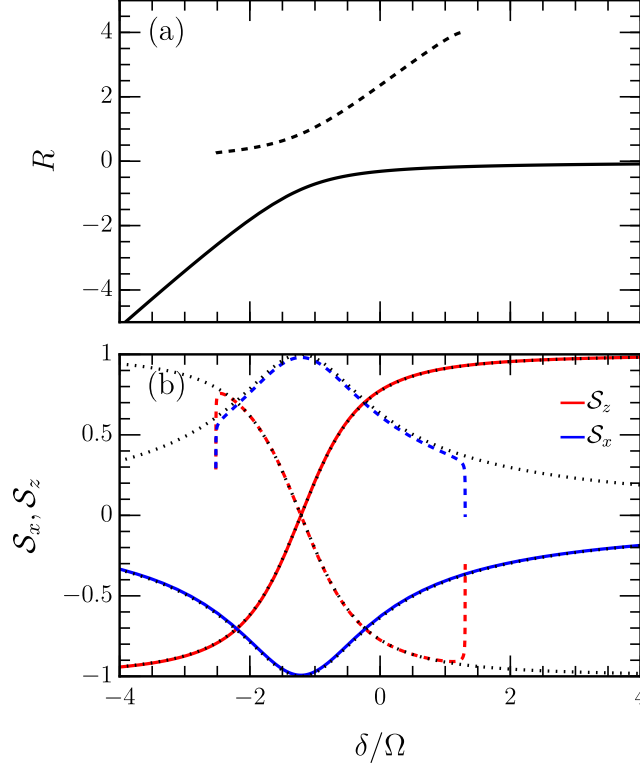


Figure S1. Properties of the hybrid bound states. (a) Ratio R versus detuning for the ground (solid line) and excited states (dashed line). (b) Magnetization vector component \mathcal{S}_z (red) and \mathcal{S}_x (blue) for the ground (solid line) and excited states (dashed line). The dotted-black lines show the magnetization obtained from the effective Hamiltonian (S22). The bare scattering lengths are $(a_{13}, a_{23})\sqrt{2m_r\Omega} = (0.6, 0.8)$ as in Fig. 3(c) of the main text.

In position space, the Fourier transforms of (S18), i.e., the two components entering the wave function in Eq. (S10), take the forms

$$\Phi_1(r) \propto \frac{\mathcal{C}}{r} \left[e^{-r/l_-} (c^2 - csR) + e^{-r/l_+} (s^2 + csR) \right], \quad (\text{S20a})$$

$$\Phi_2(r) \propto \frac{\mathcal{S}}{r} \left[e^{-r/l_-} (s^2 - cs/R) + e^{-r/l_+} (c^2 + cs/R) \right], \quad (\text{S20b})$$

respectively, where $l_- = 1/\sqrt{2m_r\epsilon}$ and $l_+ = 1/\sqrt{2m_r(\epsilon + \epsilon_+ - \epsilon_-)}$. Interestingly, we can observe that the new hybrid bound states exhibit two characteristic localization lengths l_{\pm} , which is due to the presence of the two scattering continua for lower and upper dressed particles. We also note that the two-component nature of the hybrid wave function (S20) gives rise to a radially dependent pseudospin texture.

The knowledge of the wavefunction allows us to access some properties of the hybrid bound states as shown in Figure S1 for the set of scattering lengths used in Fig. 3(c) of the main text. Panel (a) shows the ratios R (S17) and we see that they have opposite signs for the excited and the ground states. This tells us that the two hybrid bound states are made up of bare dimers that are in- and out-of-phase, respectively. In panel (b), we plot the magnetization vector components obtained from the bound-state wavefunction using

$$\mathcal{S}_z = \frac{\sum_{\mathbf{k}} \langle \psi | \hat{f}_{\mathbf{k}1}^\dagger \hat{f}_{\mathbf{k}1} - \hat{f}_{\mathbf{k}2}^\dagger \hat{f}_{\mathbf{k}2} | \psi \rangle}{\sum_{\mathbf{k}} \langle \psi | \hat{f}_{\mathbf{k}1}^\dagger \hat{f}_{\mathbf{k}1} + \hat{f}_{\mathbf{k}2}^\dagger \hat{f}_{\mathbf{k}2} | \psi \rangle}, \quad (\text{S21a})$$

$$\mathcal{S}_x = \frac{\sum_{\mathbf{k}} \langle \psi | \hat{f}_{\mathbf{k}1}^\dagger \hat{f}_{\mathbf{k}2} + \hat{f}_{\mathbf{k}2}^\dagger \hat{f}_{\mathbf{k}1} | \psi \rangle}{\sum_{\mathbf{k}} \langle \psi | \hat{f}_{\mathbf{k}1}^\dagger \hat{f}_{\mathbf{k}1} + \hat{f}_{\mathbf{k}2}^\dagger \hat{f}_{\mathbf{k}2} | \psi \rangle}. \quad (\text{S21b})$$

These magnetization components expose the differing nature of the two hybrid bound states. Indeed, we see that the extrema of \mathcal{S}_x have opposite signs and that the slope of \mathcal{S}_z at its zero-crossing is opposite for the excited and ground

states. In addition, the dotted lines in Fig. S1(b) show the magnetization obtained using the eigenvectors of the the following effective 2 by 2 Hamiltonian

$$H_{\text{eff}} = \begin{pmatrix} -\varepsilon_{13} & \frac{\Omega}{2} \\ \frac{\Omega}{2} & -\varepsilon_{23} + \delta \end{pmatrix}, \quad (\text{S22})$$

whose eigenvalues correspond to Eq. (13) of the main text. We see that the magnetization obtained from the effective model is very accurate for the ground state while it is only accurate at small detunings for the excited state. Indeed, the effective model (S22) does not account for the presence of the scattering continuum and its results are only reasonable when the bound states are well separated from it.